Hydrogen retention in beryllium nitride.

A. ALLOUCHE*

Physique des Interactions Ioniques et Moléculaires,

CNRS and Aix-Marseille Université (UMR7345),

Campus Scientifique de Saint Jérôme, service 242,

13397 Marseille Cedex 20 - FRANCE

M. OBERKOFLER

Max-Planck-Institut für Plasmaphysik

Boltzmannstr. 2, 85748 Garching, GERMANY

M. KÖPPEN, CH. LINSMEIER

Forschungszentrum Jülich GmbH, Institut für Energie- und Klimaforschung – Plasmaphysik, 52425 Jülich, Germany

E-mail: alain.allouche@univ-amu.fr

Abstract:

The valence band density of states of bulk beryllium nitride (alpha-Be_3N_2) and the solvation energy of hydrogen atoms in this nitride is herein studied using the generalized gradient approximation density functional theory. The DOS is compared to photoelectron spectroscopy investigations of nitrogen-implanted beryllium. The presence of defects (atomic vacancies) was taken into consideration in the calculations on the trapping of deuterium. The barriers of activation for hydrogen atom diffusion in the bulk and from the defect were calculated and compared to their values in pure beryllium metal and in beryllium oxide. Some consequences regarding the effects of nitrogenation of beryllium as a plasma-facing material in nuclear fusion devices are eventually proposed.

I. Introduction

Beryllium is planned to be used as a plasma-facing material for the international nuclear fusion experiment ITER and hence will be subjected to hydrogen isotopes deuterium and tritium escaping from the magnetically confined plasma. Therefore, hydrogen atom implantation and release in beryllium are vital issues that have been the focus of many investigations [1]. On the other hand seeding of impurities in the plasma is often used in tokamak experiments for various purposes. In particular, the absence of carbon in modern divertor concepts makes radiative cooling by nitrogen seeding mandatory to reduce the power flux. Thus, puffing of nitrogen reduces the divertor temperature [2,3].

Hence, understanding the interaction of nitrogen with beryllium is of great importance [4]. It has been shown that some part of the injected N_2 will be transported to the main chamber wall and deposited on the beryllium cladding to form a stable nitride layer. Furthermore, N can also be co-deposited with Be eroded from the main wall. The first potential problem is that the insulating nature of the nitride layer could increase detrimental arcing. The next problem is that nitration influences the retention of hydrogen isotopes in the material in a way and amplitude that are not well understood [5] Experiments on hydrogen release from this material have been conducted by various groups and notably at the PISCES-B facility [6]. It was observed that beryllium bombardment with energetic deuterium and nitrogen brought about the formation of mixed Be_xN_y compounds. Comparison between nitrided and un-nitrided samples is lead through thermal desorption measurement of deuterium retention.

The understanding of desorption implies understanding the fundamental processes of diffusion and trapping in the material. Elevated temperatures lead to diffusion of deuterium atoms in the bulk as interstitial atoms to reach the crystal surface where they can recombine and desorb. During diffusion they can be trapped into crystal defects, especially atomic vacancies produced by atom displacements (Frenkel pairs).

Wide band-gap semiconductors such as metal nitrides have also attracted considerable interest in recent years because of their wide-ranging technological applications in blue to UV light-emitting diodes and laser diodes [7]. Only a small number of papers has been devoted to ab initio calculation of the electronic structure

and properties of beryllium nitride; they all detail the electronic structure of the perfect crystal [8,9,10,11,12,13] except Lange et al. [14] who deal with the similar problem of hydrogen-containing point defects in Mg_3N_2.

The paper is organized as follows: section II provides details on the DFT method and the results it yields on the geometry and electronic structure of Be_3N_2, as well as a comparison to X-ray photoelectron spectroscopy (XPS) measurements in the valence band. Section III relates to the interstitial hydrogen diffusion. Section IV deals with atomic vacancy reactivity toward hydrogen and section V with the crystal surface structure and reactivity. Discussion and conclusions are proposed in Section VI.

II. Computational details and electronic structures.

The calculations are performed within the framework of the spin-polarized gradient-corrected density functional theory (DFT) using the Perdew-Burke-Ernzerhof functionals (PBE [15]) and including a semi-empirical pairwise London damped dispersion correction (PBE-D2 [16,17]). A plane-wave basis set was used with an energy cutoff of 32 Rydberg (435 eV); the ionic core potential was modeled using Vanderbilt ultrasoft pseudopotentials. The pseudopotentials were taken from the Quantum-Espresso library [18], and they were discussed in detail in a previous paper [19]. Integration in the first Brillouin zone was performed using the 6x6x6 k-points Monkhorst-Pack sampling for the bulk and 6x6x1 points for the surfaces.

The interaction energy (or dissolution energy) of a hydrogen atom with the beryllium nitride bulk (clean or defective) is defined as:

$$\Delta E_H = [E(Be_nN_m+H) - E(Be_nN_m) - 1/2\ E(H_2)]$$

eq. 1

where $E(Be_nN_m+H)$ represents the total system (clean or defective) energy and $E(H_2)$ the energy of the hydrogen molecule calculated in the same unit cell.

The temperature correction applied to the DFT energies is evaluated through calculation of the Helmholtz free energy, which is also the Gibbs free enthalpy of the

system, when the pressure and volume variations are neglected:

$$G(T) = E^{el} + E^{vib} - TS^{vib} + PV$$

eq. 2

E^{el} is the DFT electronic contribution, E^{vib} and S^{vib} are vibrational contributions to the total energy and entropy, respectively; and T, P and V are temperature, pressure and volume. When the P and V variations are neglected and T=0K $G(0) = E^{el} + E^{vib}$ is known as the Zero Point Energy; hereafter, the energies given without any other specification must be understood as ZPE-corrected PBE-D2 free energies, no further temperature adjustment will be proposed.

The stationary state structures were optimized using the damped molecular dynamics algorithm implemented in the Quantum-Espresso package. All the atoms were included in the optimization procedure, without any geometry or symmetry constraint. The activation energies for trapping, detrapping and diffusion are evaluated using the Nudged Elastic Band (NEB) algorithm [20,21,22]. The NEB calculations provide the three PBE-D energies (ΔE_{PBE}) for the initial and final configurations as well as for the transition state. ZPE correction is further added using eq. 2.

Under normal pressure the beryllium nitride has two phases, alpha and beta. The α-phase (anti-bixbyite type) is stable between 20 and 1200 °C, it is a cubic structure with symmetry space group Ia-3 (206), and lattice parameter of 8.145 Å [8]. The unit cell includes 80 atoms. It is constituted as an A-B-A-C stacking (Figure 1). Layer A is only constituted of beryllium (12 atoms). Two types of nitrogen atoms are identified in layer B, hereafter named N^{α} (4 atoms) and N^{β} (8 atoms). They are all in the same crystal plane. Layer C displays the same total number of N atoms, but now they are all identical (N^{β} type) and no more strictly coplanar. The chemical environment of the various nitrogen atoms is therefore different according to the atom type, for instance N^{α} has six Be neighbors, all at the distance of 1.752 Å. N^{β} also has six Be neighbors but distributed by pairs at 1.697, 1.761 and 1.794 Å. As a consequence, and a priori, the nitrogen atoms' chemical reactivity should differ accordingly and will be analyzed later.

The PBE-D2 optimized lattice parameter is 8.028 Å which underestimates the experimental value of 1.4 %. This underestimation is partly due to the GGA functional

parameterization and partly to the London-type correction since the pure PBE result yields 8.076 Å. Moreno-Arena et al. [8] found 8.155 Å by means of an all-electron Hartree-Fock calculation, without electron correlation correction. Mokhtari et al. [9] found 8.155 Å using FP-LAPW calculations within PW-GGA.

The total and partial densities of states (DOS) are displayed in Figure 2. Beryllium contribution is predominant in the lower part of the conduction band close to the Fermi level. The valence band is split into two parts, the lower sub-band below -15 eV is mostly constituted of N(*2s*) and Be(*2p*) and Be(*2s*) orbitals. The higher sub-band is formed of N(*2p*), Be(*2p*) and Be(*2s*) orbitals. The respective contributions of the *2s* and *2p* beryllium orbitals are similar in the two sub-bands. A more detailed analysis evidences that the individual contributions of each *2p* orbital are identical (not shown in Figure 2), which clearly indicates that the Be atom orbitals are combined according to the sp3 hybridization model and that the cohesion of the crystal is insured by the combination of these hybrid orbitals with the *2p* nitrogen orbitals.

The GGA functionals are well known to provide poor estimation of the electronic band gaps in ionic systems; this problem has been extensively discussed in the past [23]. In the present case the direct band gap at the Γ point can be approximated to 3.25 eV from the total DOS structure. This value is in good agreement with the experimental value of the optical band gap of 3.8 eV [10].

The N^{α} and N^{β} atoms contributions to the valence band are slightly but definitely different in the interval above -10 eV, in agreement with Orhan et al. results [13], this tends to prove that their chemical behaviors must differ even if not dramatically.

The Bader-Voronoi electron density analysis indicates a total atomic net charge of -0.46 e^- for N^{α} and -0.44 e^- for N^{β}, the beryllium net charge being equal to +0.30 e^-, not very different from the Löwdin scheme results, respectively -0.38, -0.36 and +0.28 e^-. For the record, the beryllium Löwdin net charge in BeO is +0.26 e^- [24], hence beryllium nitride as well as beryllium oxide must be considered as covalent-ionic crystals. This result is further confirmed by the all-electrons calculation published by Moreno Armanta et al. [8] giving a net charge of 0.65 e^- for beryllium as substantiation that beryllium nitride is far from an ideal ionic crystal [11].

Electronic Density of States (DOS) and comparison with XPS valence band

In order to check the validity of the DFT simulations, the theoretical DOS are compared in the following to experimental XPS spectra of the valence band binding energy region and involved core levels. The spectra have been recorded along progressive implantation of nitrogen in beryllium samples up to the final beryllium nitride material.

XPS spectra are acquired using two different setups: A dedicated XPS setup based on a PHI ESCA 5600 ('XPS apparatus' described in [25]) and the multi-technique experiment ARTOSS (fully described in [26]). The binding energies in all spectra are calibrated to the Au 4*f*7/2 peak at 84.0 eV.

Polished quadratic, polycrystalline Be samples with a side length of 10 mm from *MaTecK* with a bulk purity of at least 99 % are used. To remove surface contaminations and remaining impurities the samples are cyclically cleaned by sputtering with Ar^+ at 3 keV and annealing at 770 K for 30 min. After the cleaning procedure negligible amounts of oxygen are visible in the survey spectra of ARTOSS (Figure 4a). In the XPS apparatus no oxidic beryllium can be identified in the high resolution spectra of the beryllium region (Figure 3a), but small remains of implanted argon from the cleaning procedure are visible in the survey spectrum (not shown).

In a previously cleaned Be sample nitrogen ions are implanted with an acceleration voltage of 3 kV and under an angle of 45°. Oberkofler et al. have shown, that the saturation limit for the N-implantation in Be is at an upper estimate of 1.8×10^{18} N cm^{-2} [27]. Considering this upper limit, N fluences above 5×10^{17} cm^{-2} are chosen to saturate the samples. According to the survey spectrum the composition of the sample surface after N saturation equates roughly to 60 % Be and 40 % N in both experimental setups. Thus the ratio of Be_3N_2 is reached and no further implantation is necessary. At these nitrogen fluences no oxygen signals are present in the XPS spectra.

In Figure 3 the Be 1*s*, N 1*s* and valence band (VB) spectra recorded with the XPS apparatus are shown. The black spectra of the Be 1*s* and VB regions are recorded directly after the cleaning procedure and before N implantation. In the Be 1*s* region only one peak originating from metallic Be at a binding energy (BE) of 111.8 eV is visible and in agreement with literature (e.g. [28,29,30, 31,32]). No BeO or other Be-containing

compounds can be seen in this spectrum. The sample is oxygen free. In the VB spectrum of the clean sample a very strong signal can be seen at BE from 11.7 to 6.7 eV with a maximum at 8.8 eV (see black curve in Figure 3c). This signal is attributed to implanted Ar since this spectrum is recorded directly after sputter cleaning without annealing in between. At smaller binding energies from 6.7 eV onwards the signal intensity remains at a low level until the Fermi edge reflecting the metallic character of Be.

After irradiation with a N fluence of 5.9 x 10^{17} cm^{-2} the peak in the Be 1*s* region (Figure 3a) is shifted by +1.4 eV to 113.2 eV. A clear broadening of the signal is visible, comparable to BeO-signals. In the N 1*s* region (Figure 3b) one peak is visible at 397.0 eV. In the VB region (Figure 3c) we can see clearly the change from a conductor to an insulator: Between the Fermi edge and 2.0 eV below no intensity can be observed. A second local minimum is observed at a binding energy of 11.8 eV, approx. at 1.2 eV higher binding energies than in the calculations. In between a broad peak like a crest is observed. The structure of the signal as well as the upper limit of the measured intensity at 2.0 eV are in very good agreement with the DOS of the presented DFT-calculation [Figure 5].

To check the influence of ion damage induced by the implantation the sample is annealed at a temperature of 520 K to form the thermodynamically stable beryllium nitride phase, free from ion damage. After annealing shifts in all three relevant spectral regions are observable. In both core level spectra peaks are shifted towards higher binding energies: In the Be 1s-region the signal is shifted by 0.6 eV to 113.8 eV. This comes close to the value of 114.0 eV found by Soto et al. for Be_3N_2 [10]. The N 1*s* peak shifts also by 0.6 eV to 397.6 eV. In the VB-region, the measured intensity is shifted towards higher binding energies. The crest ranges from 2.1 eV to 12.6 eV.

Figure 4 shows XPS spectra recorded at the ARTOSS apparatus. These were recorded after tempering of the sample to 1000 K, which leads to outgassing of the Ar implanted in the cleaning procedure. This explains the absence of the peak in the valence band region around 8.8 eV that was observed at the XPS apparatus (Figure 3c). The appearance of the band gap is not clearly visible in figure Figure 4b due to the poor resolution and statistics of these spectra. The spectrum of clean Be (blue curve) shows no notable features. After implanting nitrogen with a fluence of 3.0 x 10^{16} cm^{-2} (red

curve) two features emerge: One feature between 3.0 and 10.6 eV and the second feature between roughly 15 and 21 eV. These features gain intensity with increasing N fluence. The cyan curve shows the spectrum after N implantation of 1.8 x 10^{18} cm^{-2} Thus, these features are clearly attributed to implanted nitrogen. This observation agrees with the structure present between 16 eV and 19 eV (Figure 4) the DOS from the DFT simulations.

In conclusion we have shown with the core level spectra shown in Figure 3, that we synthesized Be_3N_2. The DOS calculated by DFT and the valence band spectra are in reasonable agreement. Both are constituted by two significant features. The first one lies between -2.2 to -3.0 and -10.6 to -11.8 eV for XPS and between -2.0 and -10.6 eV for DFT. The second feature begins at roughly -14 eV for XPS and is slightly shifted in the DFT spectra, where it appears between -15.3 and -19.6 eV. The peak maximum is also shifted: -18.0 eV (XPS) compared to -16.4 (DFT). Between these two structures, the simulation shows a gap from -11 to -15 eV. This also corresponds quite well to the region of low intensity in the XPS spectra between -11 and -14 eV. We therefore can conclude that all features calculated by DFT are also found and reproduced in the experiment and can be compared within the experimental uncertainties.

Atomic vacancies

The good representation of the electronic structure of the material is very important in modeling the reactivity of an atomic vacancy. In pure ionic crystals such as MgO or ZnO for instance, the vacancy can result from a missing ion, O^{-2} or O^{-}, therefore this vacancy is charged and its reactivity is a function of this charge [23,33]. This approach becomes more questionable when the solid is not purely ionic. In order to clarify the matter we propose to quantify the transfer of charge induced by the creation of an atomic vacancy, with the total number of electrons remaining constant. To this end, we made use of a larger crystal cell (1x1x2, 160 atoms) including a Frenkel pair V_{Be}+Be_i or V_N+N_i [34].

The goal is to compare the charge variations of atom X_n (X=N,Be), ΔQ_n =

$Q_n(V_X)$ - $Q_n(V_X+X_i)$ where $Q_n(V_X)$ is the charge of X in the cell containing only the vacancy and $Q_n(V_X+X_i)$ the same cell containing the total Frenkel pair. The distance between the vacancy and the interstitial is 6.23 Å for the Be pair and 7.41 Å for the N one. The ΔQ_i are negligible in $V_{Be}+Be_i$ since they range from -0.07 to +0.04 e^-.

They are more important in V_N+N_i, as transferring a more electronegative atom clearly induces a larger polarization of the system, however the maximum/minimum charge transfers are 0.11/-0.10 for the beryllium atoms, and 0.21/-0.10 all atoms considered. The 80 Be atoms carry a total amount of 164.84 e^- in isolated V_N and 165.07 e^- in $V_N + N_i$, the total defect of charge is 0.23 e^-. Nevertheless for the purpose of vacancy reactivity we must focus our attention on the vicinity of the nitrogen vacancy. These data are summarized in Table 1 where it can be noticed that the larger variations are ±0.1 e^-. Given the already large number of atoms of these working cells, it was hardly possible to extend their dimensions in order to achieve convergence, Sofronov et al. showed that this task is very difficult [34], but qualitatively and within the limits of the method, this justifies that only neutral atomic vacancies will be considered in this paper without forgetting that some of them could eventually become charged.

III. Trapping and diffusion of an interstitial hydrogen atom

In the first model we considered the hydrogen atom is trapped at the center of an irregular tetrahedron, between four beryllium neighbors at respectively 1.49 Å (2 Be) and 1.78 Å (2 Be); the trapping energy is 3.59 eV. The interesting point regarding the consequences on the DOS structure is that the H impurities induce the appearance of two new peaks in the valence band, one at -9.35 eV the other one right on the Fermi energy level, imparting a half-metal structure to the solid (Figure 6a) [35].

The two other trapping sites are almost equivalent, the hydrogen atom is bonded to nitrogen whatever the type, N^α or N^β, at the distance of 1.05 Å. The only minor difference lies in the trapping energies, 3.32 eV in the first case and 3.58 eV in the other case, therefore the N^α site must be considered as slightly favored (Table 2). From this

point of view, and at this level of accuracy, the two sites can be considered as identical. In both cases the trapping results in the emergence of two new peaks in the valence band at -21.1 and -12.1 eV, no contribution around the Fermi level and a doublet in the conduction band (Figure 6a); the insulating nature of the material is then maintained.

The diffusion of the hydrogen atom from the Be site to the N site occurs with an activation energy of 0.60 eV evaluated through a 21-images NEB calculation. The reverse diffusion needs to overcome a barrier of 0.41 eV. Diffusion out of a Be site to another Be site needs an energy amount of 0.66 eV whereas the N-to-N diffusion implies a barrier of 0.42 eV (Table 3).

IV. Hydrogen in atomic vacancies

Beryllium atom vacancy (V_{Be} [36]).

The lattice structure is not affected by the vacancy, whose center is located at 1.78 Å from the neighboring nitrogen atoms in lieu of 1.75 Å. The hydrogen atom gets trapped in the vacancy at a distance of 0.67 Å from the original center of the defect, bonded to a nitrogen atom (H-N = 1.04 Å). This process stabilizes the whole system by an energy of 2.67 eV: H trapping in the beryllium single vacancy is exothermic in beryllium nitride as well as beryllium oxide (Table 2) while it was endothermic in pure metallic beryllium. The consequence of this high stability is that the barrier to exit the vacancy is very high, 2.47 eV, while the reverse one is quite negligible, 0.19 eV (Figure 7a). It can be noted that this energy barrier is smaller than the total stabilization energy. In fact, this comparison is not physically significant since the trapping energy is referred to the H atom energy in the H_2 molecule, whereas the reference of the last image of the NEB calculation is H in the bulk and close to the vacancy.

Nitrogen atom vacancies (V_N).

The N^{α} vacancy can be regarded as spherical because the center of the vacancy is equidistant from its six limiting beryllium atoms, 1.81 Å. This value indicates a very small enlargement of the lattice structure since the N^{α} – Be distance is 1.75 Å. Unlike the preceding site, trapping is now endothermic, 1.22 eV. The N^{β} vacancy is less

symmetric, 2 berylliums are at 1.72 Å (1.70 Å in pure Be), 2 at 1.81 Å (1.76) and 2 at 1.85 Å (1.79). Nevertheless, the trapping energy remains the same, i.e. 1.18 eV. As a consequence the barrier of activation for detrapping was evaluated for this latter case only; it is similar to detrapping from V_{Be}, 3.42 eV and 0.17 eV for the reverse reaction. The NEB reaction path is represented in Figure 7b. The hydrogen atom goes from its position inside the vacancy to get bonded to a nitrogen atom close to V_N. The local minimum at the point ipath=7 corresponds to the interaction with two beryllium atoms limiting the vacancy.

V. Surface structures and reactivity

The slab representing the {111} surface includes 160 atoms, its two faces are identical therefore there is no dipole moment between them. The surface section is hexagonal and its dimensions are 11.36x11.36x30.0 $Å^3$ (Figure 8). Due to the large number of atoms in the cluster, ZPE correction is hardly feasible and the values reported in Figure 9 are the non-corrected PBE-D2 results. The reaction coordinate is the altitude of the hydrogen atom over the original neat cluster surface defined after relaxation of the slab. All the other coordinates (in particular X_H and Y_H) are allowed to relax freely, only the Be and N lower layers of the cluster (Figure 8) are fixed.

In approaching the surface, after a barrier of 0.17 eV, H meets the upper beryllium layer causing the first minimum indicated by Be shown in Figure 9. For this barrier, and the others in this section, the reference is the point Z_H = 6 Å, i.e. H non-interacting with the slab surface. The energy associated to this point is very small, -0.23 eV. Then another local minimum of -0.36 eV corresponds to the interaction with the nitrogen layer (denoted by the letter N in Figure 9). These minima are not thermodynamically stable in respect to H with H_2. Nevertheless the amount of energy needed to cross the first nitride layer is 1.60 eV and leads to the local minimum at 0.49 eV where H is bonded to a nitrogen atom (distance 1.051Å); this would show that the H_i formation energy is notably smaller at the layers close to the surface than in the bulk where the trapping energy is at least 3.32 eV (Table 2).

The {001} surface was represented by a slab of 80 atoms (cell parameters 8.03x8.03x25.0 Å) with a vacuum of 13 Å, it exposes 2 nitrogen atoms and 12

berylliums. None of these sites are reactive towards hydrogen because the energy of the most stable minimum energy above N is only -0.07 eV and is higher than the hydrogen atom fixed further from the slab surface (5Å).

The 8.03x11.36x25.0 Å³ slab containing 160 atoms assumed to represent the {110} surface, proved to be unstable and this system was the last we investigated after no more fruitful attempts.

VI. Discussion and conclusions

To summarize our contributions to the study of beryllium-based materials reactivity towards hydrogen atoms retention, it was found that the activation barriers for H mobility extend from 0.41 to 0.69 eV in the bulk, which is in the same range as in the pure metal but slightly smaller than in the oxide (Table 3); this, in particular, explains that when growing on a pure beryllium substrate the nitride layer does not act as a diffusion barrier for out-diffusing hydrogen isotopes [5]. On the contrary the barriers to trapping in all the types of atomic vacancies in Be_3N_2 are negligible, which was not the case for the other materials. On this point as well as on the other properties herein investigated, the difference between the two types of nitrogen atoms (N^{α} and N^{β}) is not significant, this point deserved to be confirmed although it had already been mentioned by Lange et al. for the similar Mg_3N_2 system [14].

Studying desorption of a gas from a solid implies evaluating the role of the surfaces as a first step: the surface could offer a barrier to desorption that could be the rate-limiting process depending on its value. Although our investigations on the beryllium nitride surfaces cannot be exhaustive, in view of the results reported above it can reasonably be assumed that the surfaces are of little importance in the physics of hydrogen desorption from the Be_3N_2 crystal.

On another hand, Figure 9 shows that the surfaces offer little opposition to hydrogen penetration since the barrier they form is rather small and the dissolution energy is markedly smaller in the first layers of the slab than in the bulk. On this particular point Table 2 indicates that the interstitial hydrogen formation in the nitride material is intermediate between the pure metal and the oxide. Its mobility, however, is

slightly easier.

Hydrogen trapping close to the anionic vacancies (N,O) is largely endothermic in both Be_3N_2 and BeO materials, but it is strongly exothermic in V_{Be} and more so for the nitride than for the oxide, the defective structure energy taken as reference. In any case the barriers to get trapped in the vacancies are very small, if not negligible. There is no contradiction between the low barrier to inclusion in the vacancies and the stated endothermicity, H in a vacancy is always more stable than H_i as evidenced by Figure 7. Hence it appears from Table 3 that hydrogen atom diffusion in the beryllium nitride bulk is very easy (less than 0.69 eV) and that if, during diffusion, H meets a vacancy, the mechanism is barrierless and almost irreversible since the barrier to exit the defect is at least 2.47 eV (V_{Be}) or 3.42 eV (V_N).

For lack of data concerning beryllium and its derivatives, magnesium is often proposed as an alternative in laboratory experiments to address the problem of the toxicity of Be [37]. This paper contributes to the discussion since it once more highlights the difference in the reactivity of these two elements: in Mg_3N_2 it was indicated [14] that the interstitial H prefers the formation of amide-like N-H complexes, it is not the case for the beryllium nitride. Only in V_{Be} does H form a strong chemical bond with N. In the case of N-bonded H_i, it is worth noting that their formation energies are smaller by a factor of 2 in Mg_3N_2 than in Be_3N_2, 1.54 to 1.62 eV for the first system toward 3.32 to 3.58 eV for the second. This further evidences that magnesium can hardly be considered as a genuine substitute for beryllium.

As a conclusion, the perfect beryllium nitride solid was taken as a model in studying the influence of the nitration of beryllium as a plasma-facing material for ITER. The DFT calculations show that this option would decrease the probability of H trapping as interstitial. Nevertheless the beryllium-type atomic vacancies (V_{Be}) would constitute very stable exothermic trapping sites that would be very difficult to exit. The positive aspect is that hydrogen retention in this type of defect yields a nonzero energy carrier at the Fermi energy level transforming the insulating beryllium nitride into a half-metal reducing the risk of arcing in the fusion device.

ACKNOWLEDGMENTS

This work was carried out within the framework the European Fusion Development Agreement and the French Research Federation for Fusion Studies. It is supported by the European Communities under the contract of Association between Euratom and CEA. The views and opinions expressed herein do not necessarily reflect those of the European Commission.

The authors were granted access to the HPC resources of [CCRT/CINES/IDRIS] under the allocation i2014080509 made by GENCI (Grand Equipement National de Calcul Intensif). A large part of the work was also carried out using the HELIOS supercomputer system at the Computational Simulation Centre of International Fusion Energy Research Centre (IFERC-CSC), Aomori, Japan, under the Broader Approach collaboration between Euratom and Japan, implemented by Fusion for Energy and IAEA.

Tables

Atom type	Distance (Å)	Q in V_N isolated (a)	Q in V_N +N_i (b)	ΔQ (c)
Be	1.78	1.78	1.69	0.09
Be	1.78	1.78	1.83	-0.06
Be	1.88	1.77	1.73	0.03
Be	1.88	1.77	1.87	-0.10
Be	1.88	1.81	1.70	0.10
Be	1.88	1.81	1.81	0.004

Table 1

Löwdin charge distribution on the beryllium atoms delimiting the nitrogen vacancy V_N. (a) in the cluster including the vacancy only (b) in the cluster including the Frenkel pair (c) difference between the two models.

Site in material	Energy of formation
H_i in Be_3N_2 Be site	3.59
H_i in Be_3N_2 N^{α} site	3.32
H_i in Be_3N_2 N^{β} site	3.58
H_i in BeO	4.36
H_i in metallic Be	2.20
H in V_{Be} vacancy in Be_3N_2	-2.67
H in V_{Be} vacancy in BeO	-2.38
H in V_{Be} vacancy in metallic Be	0.44
H in V_N vacancy in Be_3N_2	1.22
H in V_O vacancy in BeO	1.61

Table 2

Hydrogen defects formation energy (in eV) calculated according to eq. 1 and compared to beryllium oxide [24] and pure beryllium [38]

Site in material	Barriers of activation	
H_i in Be_3N_2	0.41 (N to Be)	0.60 (Be to N)
H_i in Be_3N_2	0.42 (N^{β} to N^{β})	
H_i in Be_3N_2	0.69 (Be to Be)	
H_i along the {001} direction in Be	0.74	
H_i parallel to the {110} plane in Be	0.41	
H_i along the {001} direction in BeO	0.88	
H_i parallel to the {110} plane in BeO	0.70	
H in V_{Be} in Be_3N_2	0.19 (to V_{Be})	2.47 (from V_{Be})
H in V_N in Be_3N_2	0.17 (to V_N)	3.42 (from V_N)
H in V_{Be} in Be	0.58 (to V_{Be})	1.57 (from V_{Be})
H in V_{Be} in BeO	0.80 (to V_{Be})	2.87 (from V_{Be})
H in V_O in BeO	0.75 (to V_O)	3.44 (from V_O)

Table 3

Hydrogen defects diffusion: barriers of activation (in eV)

Figures

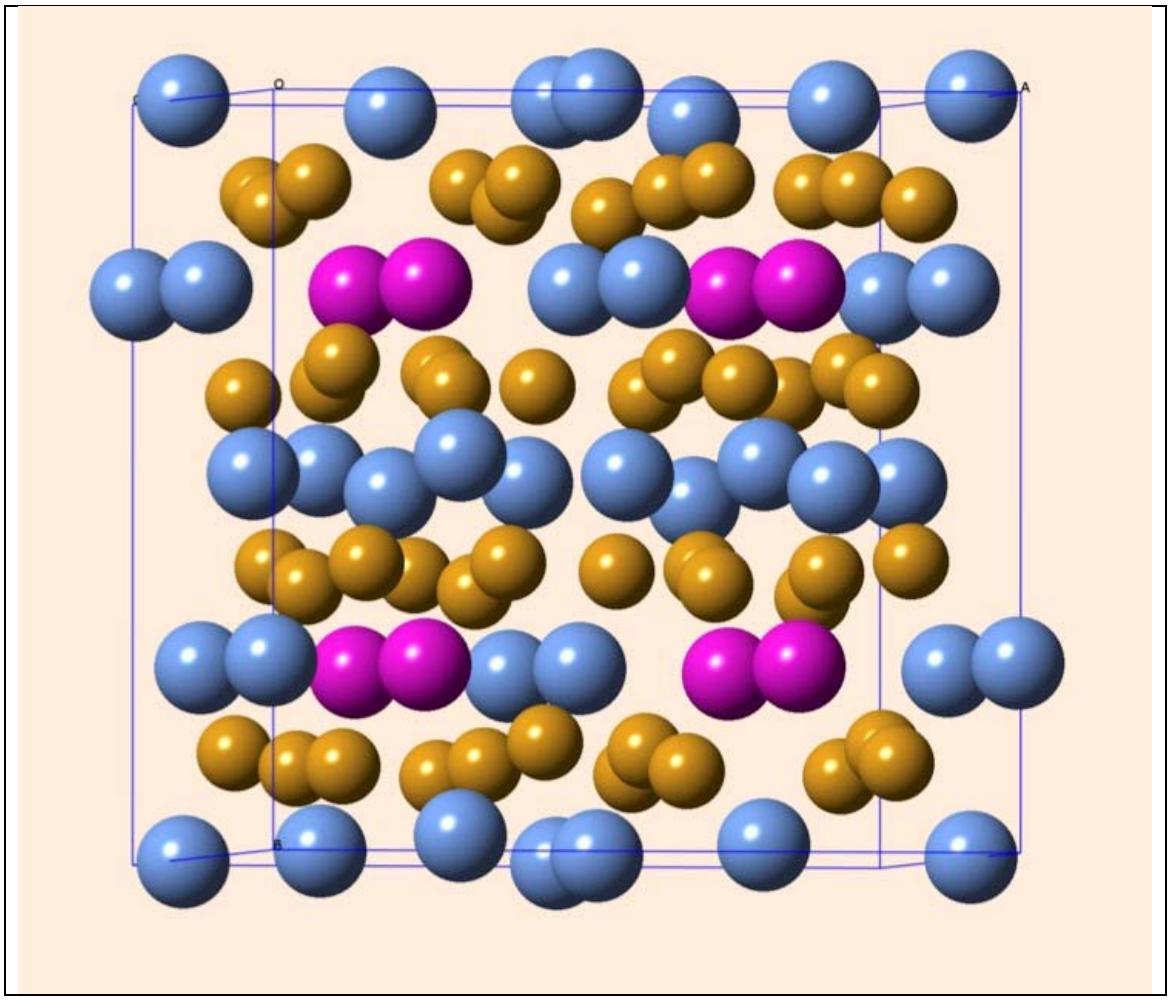

Figure 1

Unit cell of α-Be_3N_2: The beryllium atoms are in yellow color, two types of nitrogen atoms can be identified: N^{α} in purple and N^{β} in blue.

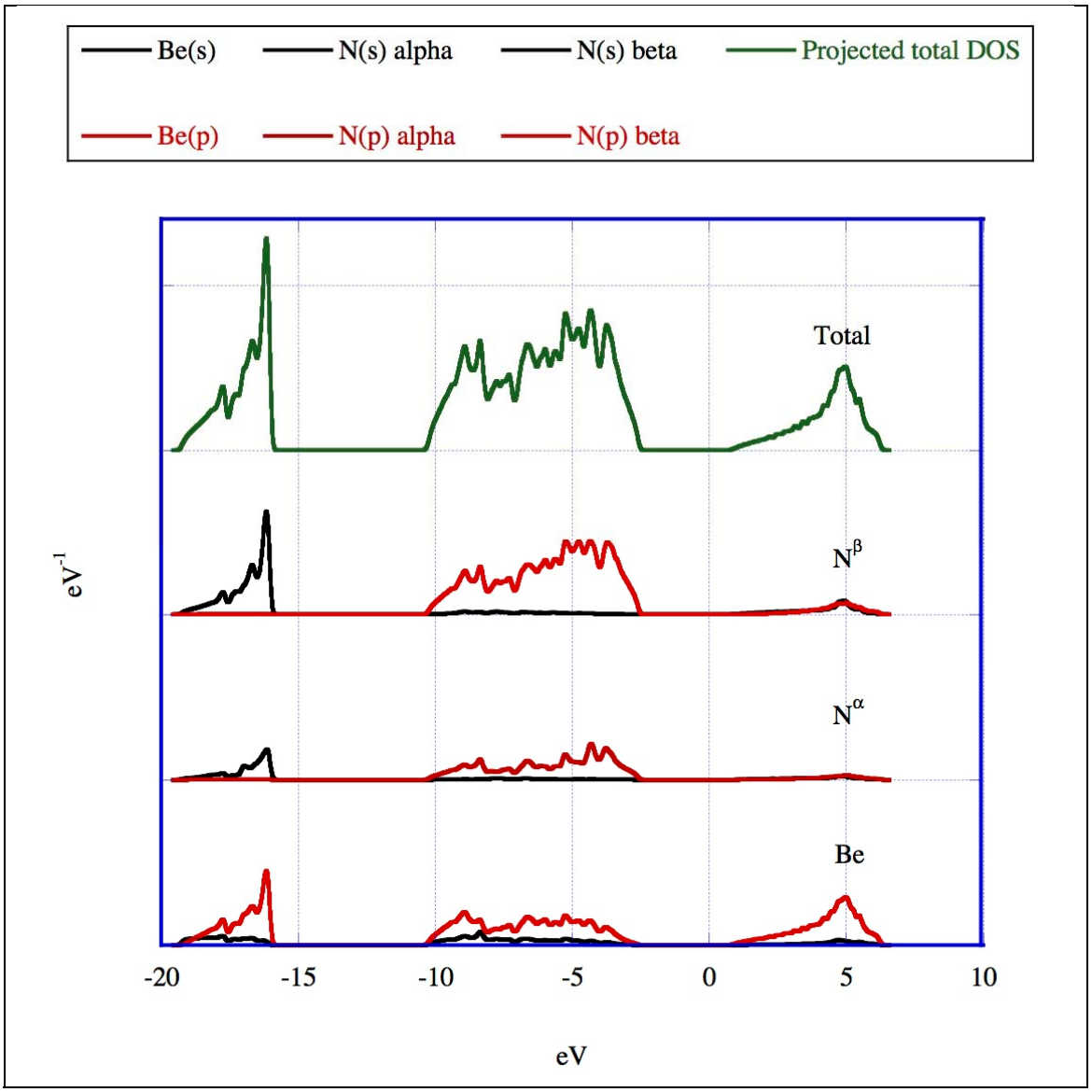

Figure 2

Total and partial density of states for Be_3N_2, the partial 2s contributions for each atom type is in black, the 2p contribution in red. The origin of energy is at the Fermi Energy level.

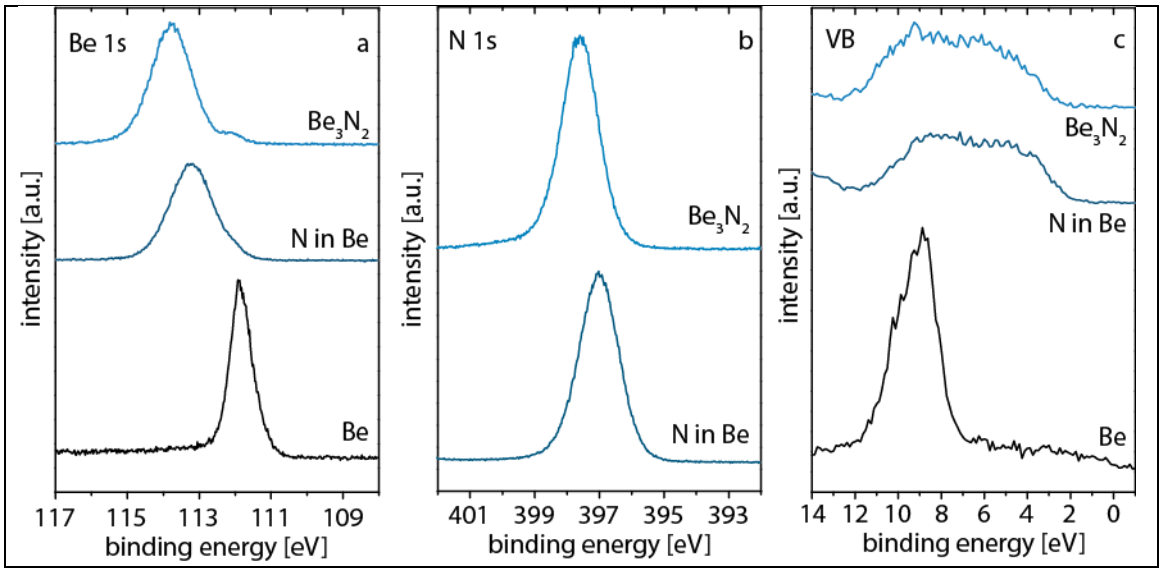

Figure 3

Core level and valence band spectra: In Figure (a) the core level spectra of the Be 1s region and in figure (b) the spectra of the N 1s region is shown. Figure (c) shows the spectra of the valence band region. The black curves show clean beryllium, the dark blue curves are recorded after N-implantation and the light blue curve after annealing.

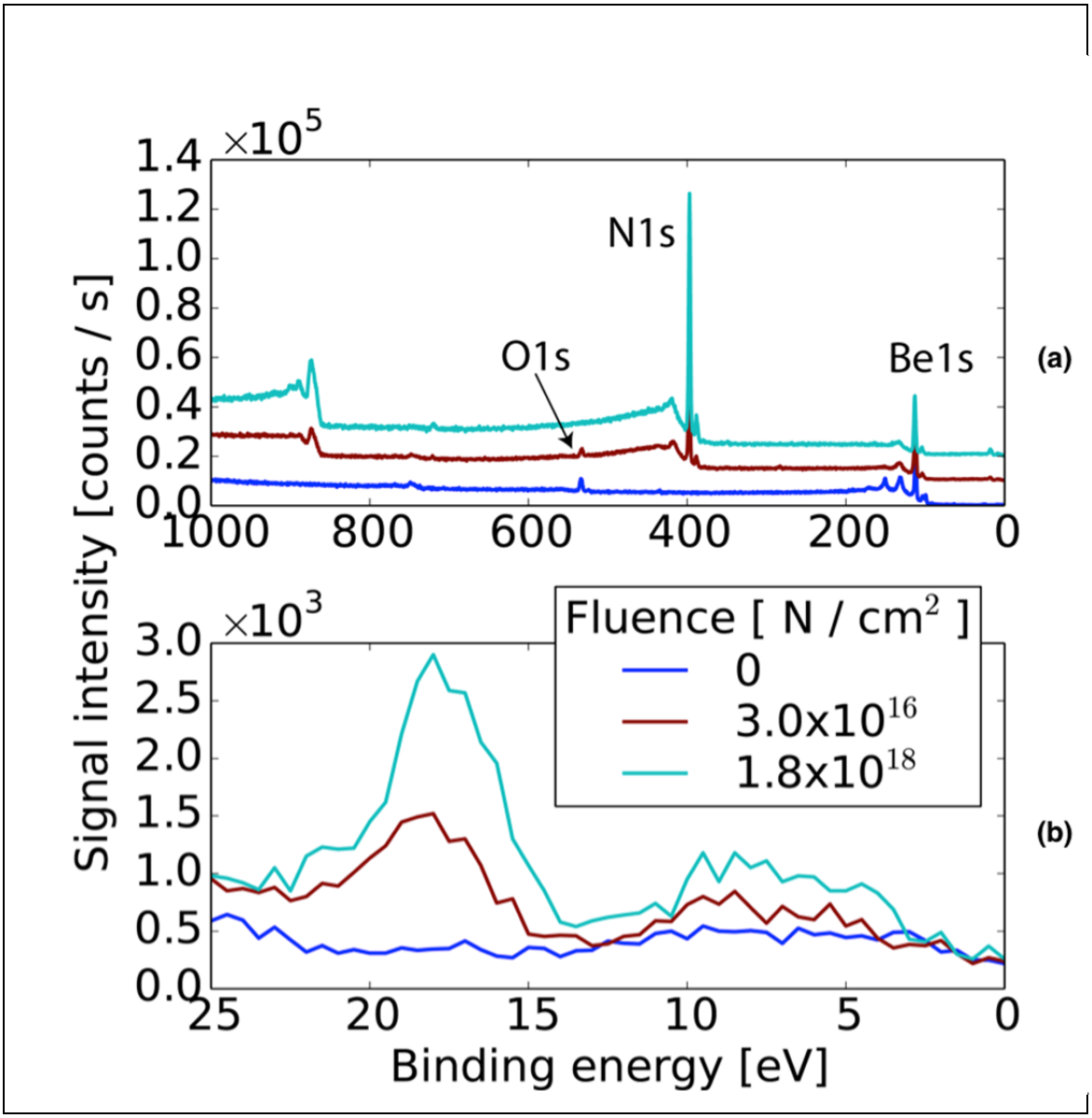

Figure 4

ARTOSS_XPS: (a) XPS survey spectra recorded at the ARTOSS apparatus on clean Be and after ion implantation of increasing fluences of nitrogen. For better visualization the spectra are successively upshifted by 10,000 counts/s. (b): Zoom-in on the valence band region.

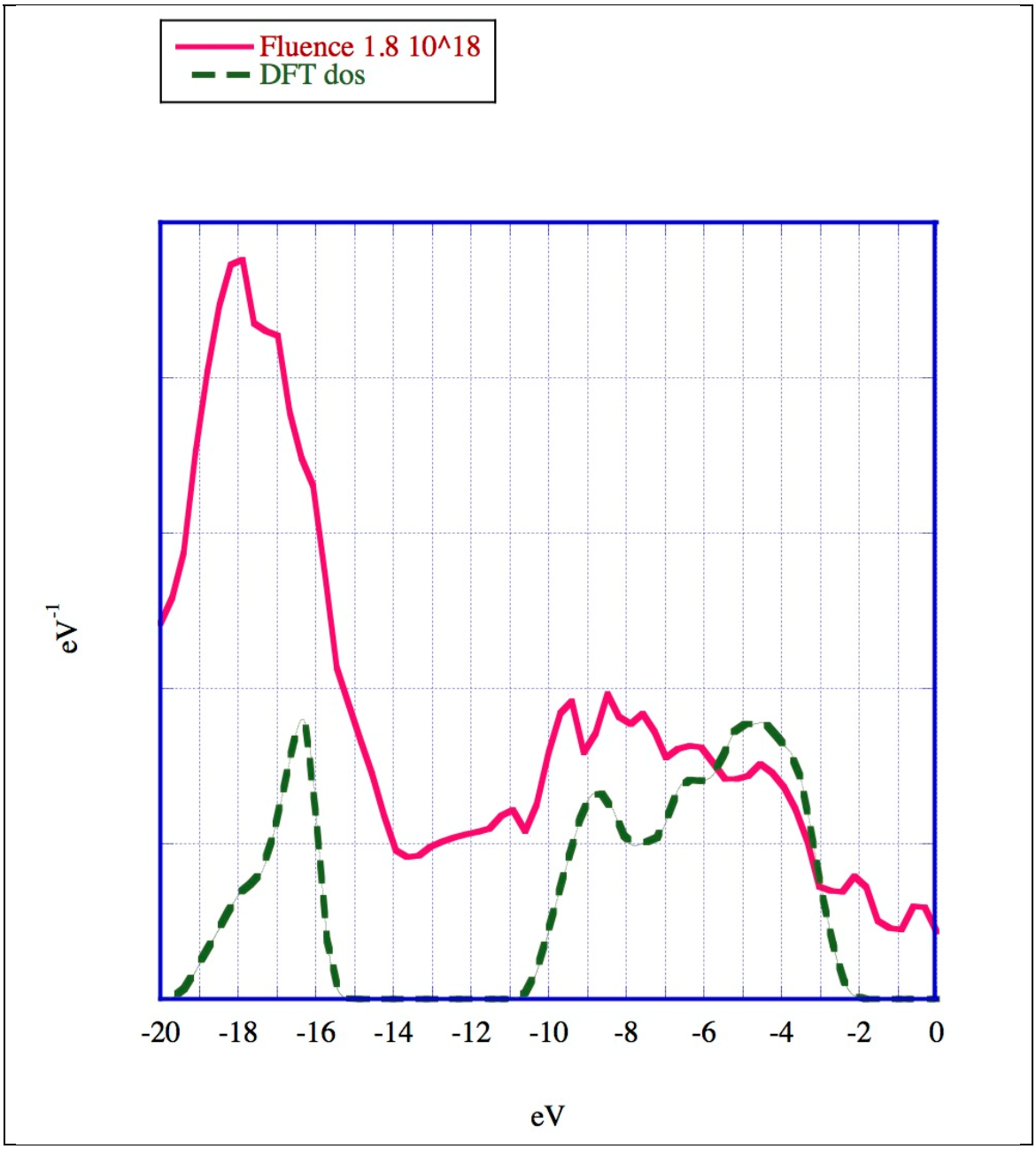

Figure 5

Comparison of the DFT density of states and the XPS spectrum in the valence band region after implantation of 1.8 10^18 N/cm^2. The XPS energies are given in negative values in respect to Figure 4.

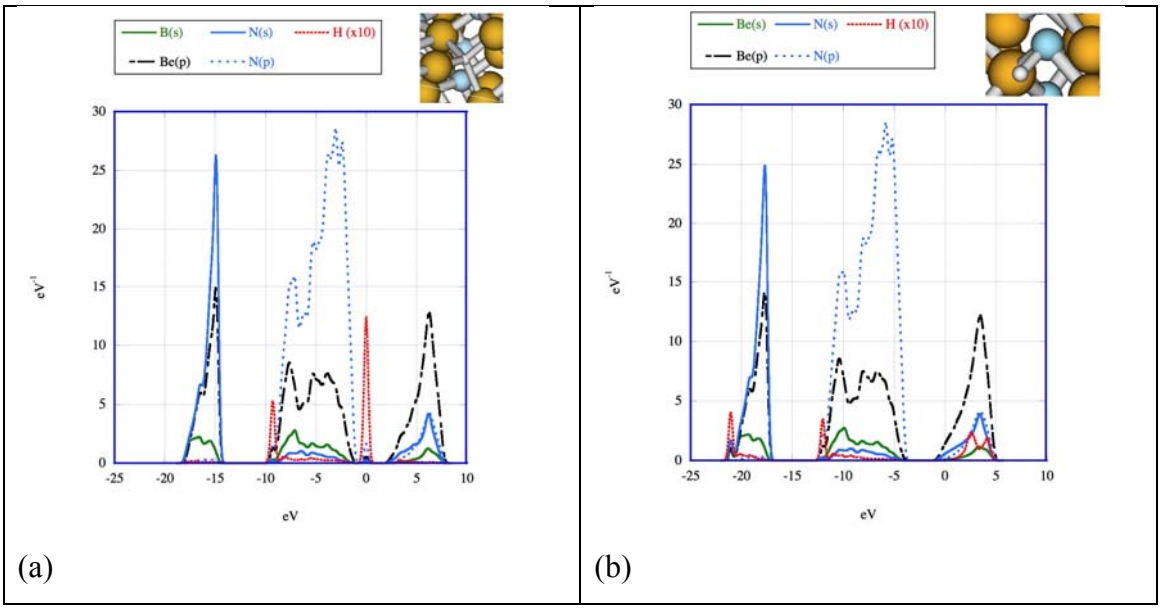

Figure 6

Be_3N_2 DOS modification induced by interstitial hydrogen atom trapping: (a) Be site (b) N site.

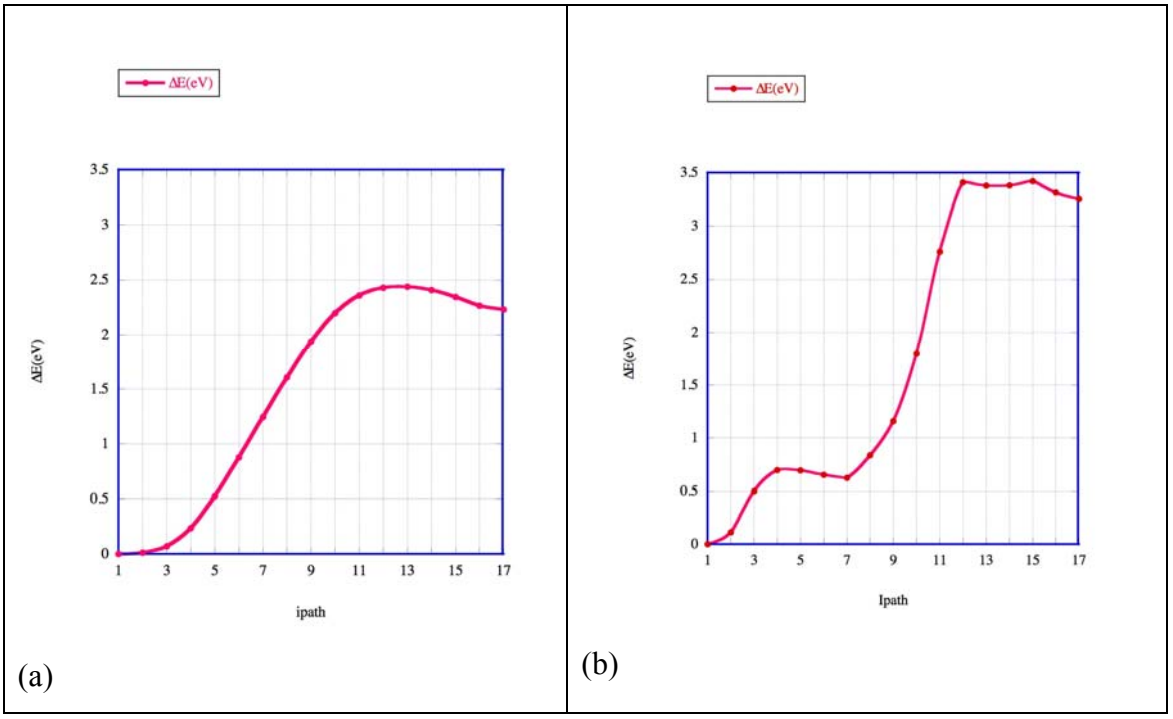

Figure 7

NEB representation of H trapping in atomic vacancies (a) V_{Be} (b) V_N: The first point (Ipath=1) is the reference energy of the hydrogen atom in the atomic vacancy, the last point corresponds to interstitial H (H_i).

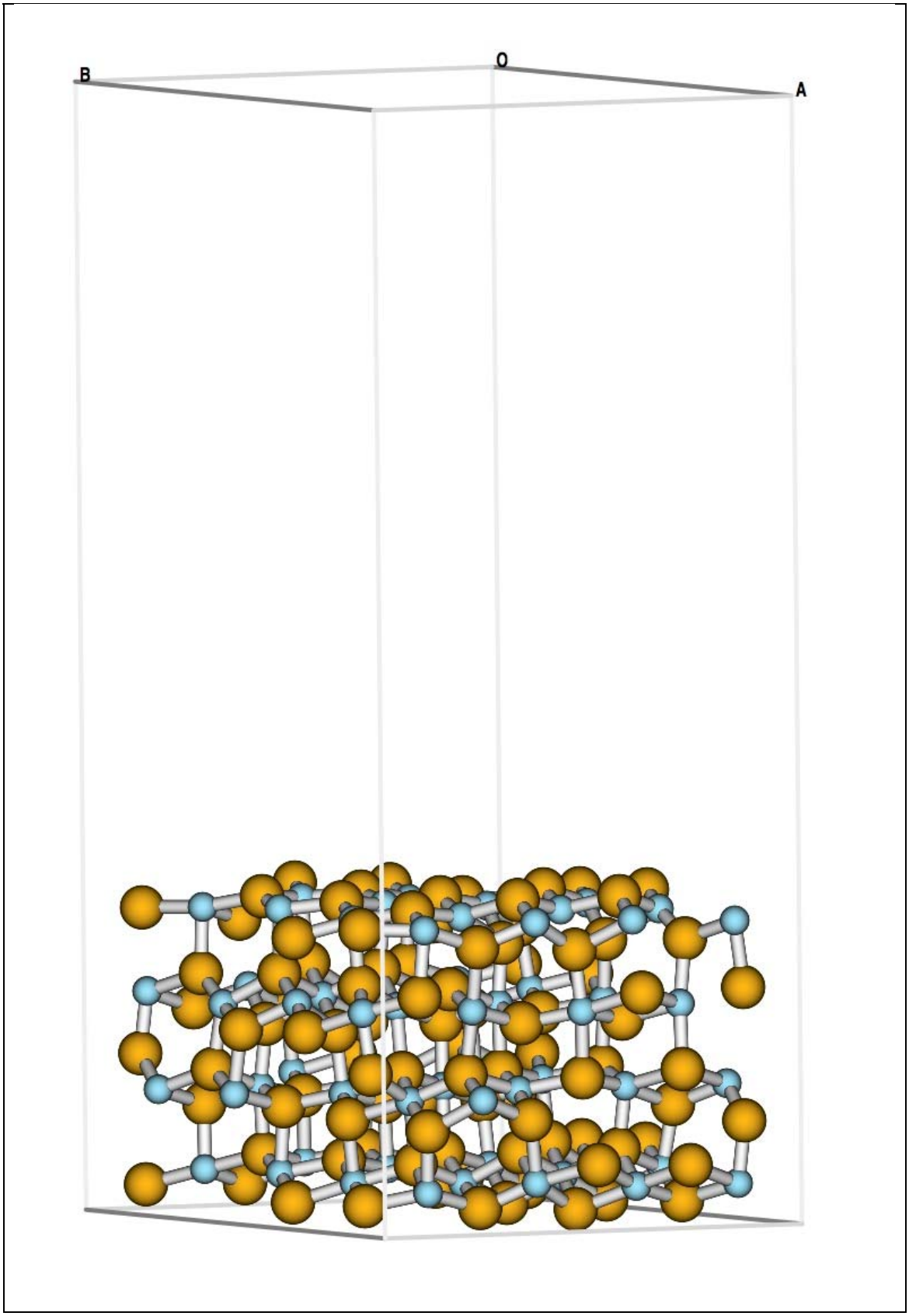

Figure 8

Structure of the Be_3N_2 {111} surface

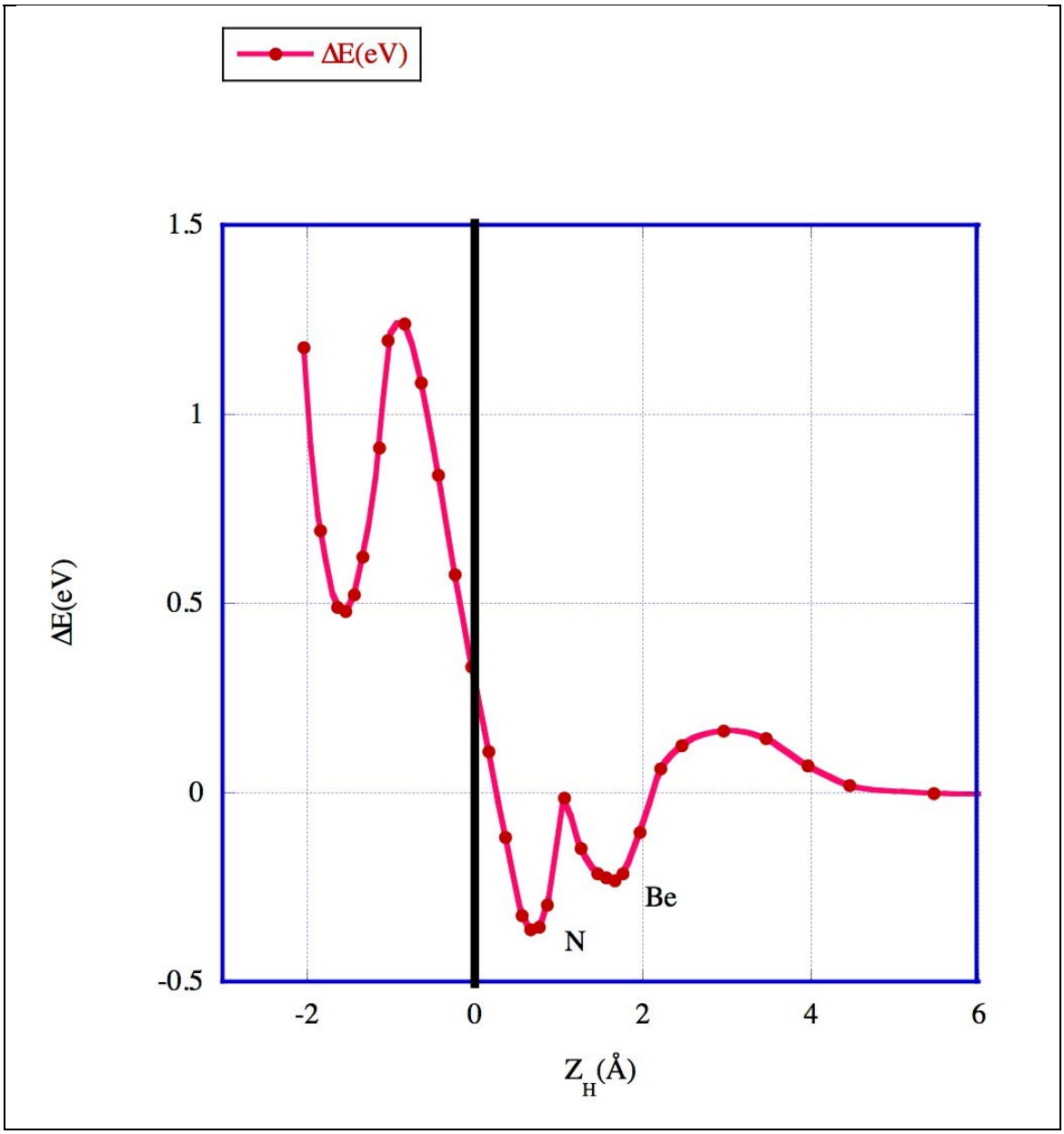

Figure 9

Potential energy surface (PES) associated to a hydrogen atom approaching the Be_3N_2 {111} surface. The reaction coordinate Z_H is the hydrogen atom altitude above the original crystal surface represented by the vertical plain line.

Reference

[1] C. H. Skinner, A. A. Haasz, V. Kh. Alimov, N. Bekris, R. A. Causey, R. E. H. Clark, J. P. Coad, J. W. Davis, R. P. Doerner, M. Mayer, A. Pisarev, J. Roth, T. Tanabe, Fus. Sci.Technol. ***54 (2008) 891.***

[2] Kallenbach et al., Journal of Nuclear Materials 415 (2011) S19–S26

[3]Van Rooij at al., Journal of Nuclear Materials 438 (2013) S42–S47

[4] A.Allouche, J. Phys.: Condens. Matter 25 **(**2013**)** 225002.

[5] M.Oberkofler, Ch.Linsmeier, Nucl. Fus. 50(2010) 125001.

[6] T.Dittmar, M.J.Baldwin, R.P.Doerner, D.Nishijima, M.Oberkofler, T.Swartz-Selinger, F.Tabares, Phys. Scr. T145(2011) 014009.

[7] R-J. Xie, H. T. Hintzen, J. Am. Ceram. Soc. 96(2013)665.

[8] M. G. Moreno Armenta, A. Reyes□Serrato, and M. Avalos Borja, Phys. Rev. B 62(2000)4890.

[9] A. Mokhtari,H. Akbarzadeh, Physica B 337 (2003) 122.

[10] G. Soto, J.A. Dıaz, R. Machorro, A. Reyes-Serrato, W. de la Cruz, Mater. Lett. 52 (2002) 29.

[11] M. G. Moreno Armenta, A. Reyes-Serrato, Comput. Mater. Sci. 21(2001) 95.

[12] M.Dadsetani, R.Beiranvand, Comput. Mater. Sci. 49 (2010)400.

[13] E. Orhan, S. Jobic, R. Brec, R. Marchanda, J.-Y. Saillard, J. Mater. Chem. 12 (2002) 2475.

[14] B.Lange, C.Freysoldt, J.Neugebauer, Phys. Rev. B 81(2010) 224109.

[15] J.P. Perdew, K. Burke, M. Ernzerhof , Phy. Rev. Lett 77 (1996) 3865.

[16] E.J. Meijer, M. J. Sprik, J. Chem. Phys. 105 (1996) 8684.

[17] S. Grimme, J. Comput. Chem. 25 (2004) 1463.

[18] P. Giannozzi, S. Baroni, N. Bonini, M. Calandra, R. Car, C. Cavazzoni, D. Ceresoli, G. L. Chiarotti, M. Cococcioni, I. Dabo, A. Dal Corso, S. De Gironcoli, S. Fabris, G. Fratesi, R. Gebauer, U. Gerstmann, C. Gougoussis, A. Kokalj, M. Lazzeri, L. Martin-Samos, N. Marzari, F. Mauri, R. Mazzarello, S. Paolini, A. Pasquarello, L. Paulatto, C. Sbraccia, S. Scandolo, G. Sclauzero, A. Seitsonen, A. Smogunov, P. Umari, R. M. Wentzcovitch, J. Phys.: Condens. Matter 21 (2009) 395502.Website: http://www.quantum-espresso.org/.

[19] A.Allouche, Phys. Rev. B, 78 (2008) 085429.

[20] E. Weinan, W. Ren, E. Vanden-Eijnden, Phys. Rev. B, 66 (2002) 052301.
[21] Y.Kanai, A.Tilocca, A.Selloni, R.Car, J. Chem. Phys. 121 (2004) 3359.
[22] G. Henkelman, H. Jonsson, J. Chem. Phys. 111 (1999) 7010.
[23] C. Freysoldt, B. Grabowski, T. Hickel, J. Neugebauer, G. Kresse, A. Janotti, C. G. Van de Walle, Rev. Mod. Phys. 86 (2014) 253.
[24] A.Allouche, Y.Ferro, Solid. Stat. Phys. In press (2015)
[25] A. Wiltner and Ch. Linsmeier, New Journal of Physics 8 (2006) 181
[26] Ch. Linsmeier Phys. Scr. T94, 28 (2001)
[27] M.Oberkofler, Ch.Linsmeier, Nucl. Fus. 50, 12 (2010)
[28] M Köppen, J Riesch, A Vollmer and Ch Linsmeier, Phys. Scr. T145, 014015 (2011).
[29] A Wiltner, F Kost, S Lindig and Ch Linsmeier, Phys. Scr. T128, 133 (2007).
[30] P. Goldstraß, K.U.Klages, Ch.Linsmeier, J. Nucl. Mater. 290-293, 76 (2001).
[31] C.J.Powell, appl. Surf. Sci. 89, 141 (1995)
[32] J.F.Moulder, W.F.Stickle, W.F.Sobol, K.D.Bomben□, Handbook of X-Ray Photoelectron Spectroscopy, [ed] J.Chastain, s.l. : Pelkin-Elmer Corporation (1992).
[33] S. C. Middleburgh, K. P. D. Lagerlof, R. W. Grimes, J. Am. Ceram. Soc., 96 (2013) 308.
[34] A.A. Sofronov, M.A. Gorbunova, Y.N.Makurin, V.S.Kiiko, A.L. Ivanovskii, J. Struct.Chem. 47 (2006) 760.
[35] I.R. Shein, M.A. Gorbuniva, Y.N. Makurin, V.S. Kiko, A.L. Ivanovskii, Int. J. Mod. Phys. B 22 (2008) 4987.□
[36] Kroger-Vink notation : F.A. Kröger, H.J. Vink, Solid State Phys. 3 (1956) 307.
[37] L. Marot, Ch. Linsmeier, B. Erena, L. Moser, R. Steiner, E. Meyer, Fus. Eng. Des. 88 (2013) 1718
[38] A.Allouche, M Oberkofler, M Reinelt, Ch Linsmeier, J. Phys.Chem. C 114 (2010) 3588.